

Cavity Quantum Electrodynamics Complete Active Space Configuration Interaction Theory

Nam Vu,^{*,†} Daniel Mejia-Rodriguez, Nicholas P. Bauman, Ajay Panyala, Erdal
Mutlu,[‡] Niranjana Govind,^{‡,¶} and Jonathan J. Foley IV^{*,†}

[†]*Department of Chemistry, University of North Carolina Charlotte, 9201 University City Blvd,
Charlotte, North Carolina 07470A*

[‡]*Physical and Computational Sciences Directorate, Pacific Northwest National Laboratory,
Richland, WA 99352*

[¶]*Department of Chemistry, University of Washington, Seattle, WA 98195, USA*

E-mail: nvu12@charlotte.edu; jfoley19@charlotte.edu

Abstract

Polariton chemistry has attracted great attention as a potential route to modify chemical structure, properties, and reactivity through strong interactions between molecular electronic, vibrational, or rovibrational degrees of freedom. A rigorous theoretical treatment of molecular polaritons requires the treatment of matter and photon degrees of freedom on equal quantum mechanical footing. In the limit of molecular electronic strong or ultrastrong coupling to one or a few molecules, it is desirable to treat the molecular electronic degrees of freedom using the tools of *ab initio* quantum chemistry, yielding an approach we refer to as *ab initio* cavity quantum electrodynamics, where the photon degrees of freedom are treated at the level of cavity quantum electrodynamics. Here, we present an approach called Cavity Quantum Electrodynamics Complete Active Space Configuration Interaction theory to provide ground- and excited-state polaritonic surfaces with a balanced description of strong correlation effects among electronic and photonic degrees of freedom. This method provides a platform for *ab initio* cavity quantum electrodynamics when both strong electron correlation and strong light-matter coupling are important, and is an important step towards computational approaches that yield multiple polaritonic potential energy surfaces and couplings that can be leveraged for *ab initio* molecular dynamics simulations of polariton chemistry.

Introduction

The field of polariton chemistry has excited the imagination of chemists, physicists, and materials scientists who have demonstrated many compelling ways that strong coupling between light and molecules can affect chemical properties and dynamics.^{1–29} The theoretical challenges in polaritonic chemistry bridge most domains of chemical physics, including *ab initio* quantum chemistry, cavity quantum electrodynamics, computational electrodynamics, statistical thermodynamics, and rate theories as pointed out by a recent review and perspective articles on theoretical advances in polaritonic chemistry.^{30–33} In this work, we introduce a method called Cavity Quantum Electrodynamics Complete Active Space Configuration Interaction theory (QED-CASCI) that provides

a variational route to ground- and excited-state polariton states and assess its accuracy against several model systems for which we can provide numerically exact benchmarks. QED-CASCI provides an important theoretical toolkit at the intersection of *ab initio* quantum chemistry and cavity quantum electrodynamics, which we will generally refer to here as *ab initio* cavity quantum electrodynamics, that should be able to inherit many of the favorable properties that have enabled CASCI to become a workhorse method in simulating *ab initio* molecular dynamics on multiple potential energy surfaces, namely smooth potential energy surfaces,³⁴ size consistent and size intensive vertical excitation energies,³⁵ the ability to formulate analytic nuclear derivatives and derivative couplings,³⁶ and the ability to formulate relatively simple corrections to incorporate dynamic correlation.³⁷

The goal of *ab initio* cavity quantum electrodynamics methodologies, in general, is to provide a detailed and rigorous description of the molecular energy eigenstates coupled to quantized photon states that are treated within the framework of cavity quantum electrodynamics. Ideally, these approaches should provide reliable accuracy across coupling regimes, i.e. spanning weak, strong, and ultra-strong coupling. There are at least two complementary approaches to this problem: so-called parameterized CQED methods and self-consistent CQED methods. The former parameterized approach involves solving two Schrödinger equations in series: a first for the molecular system alone using traditional tools of *ab initio* quantum chemistry, and the second for the coupled molecular-photon system that is parameterized by the solutions to the molecular problem.^{30,38,39} On the other hand, the self-consistent approach involves augmenting *ab initio* quantum chemistry methods to directly include coupling to photonic degrees of freedom. Such approaches have included quantum electrodynamics generalizations of density functional theory (QEDFT^{32,40–45} and QED-DFT^{46–48}), real-time^{40,41,49–52} and linear-response^{46,53,54} formulations of QED-TDDFT, configuration interaction (QED-CIS),⁵⁵ cavity QED extension of second-order Møller-Plesset perturbation theory and the algebraic diagrammatic construction,^{56,57} coupled cluster (QED-CC),^{48,58–60} variational QED-2-RDM methods,⁶¹ and diffusion Monte Carlo.⁶² To the best of our knowledge, this is the first formulation of QED-CASCI.

A central part of CASCI (and other active-space or multi-reference configuration interaction calculations) includes performing an FCI expansion within an active space defined by a number of active electrons N_{el} with all possible excitations within a number of active orbitals N_{orbs} , (N_{el}, N_{orbs}) , where just as in FCI, the number of determinants scales factorially with the number of active electrons and orbitals.⁶³ A number of algorithmic advances have pushed the limits of the sizes of these calculations. A major advance in direct CI algorithms in the 1990s due to Olsen and coworkers led to active spaces on the order of (10,10) with roughly 1 billion determinants.⁶⁴ The current state of the art in massively-parallel direct active space CI algorithms can treat active space sizes of (22,22) with roughly 1 trillion determinants.⁶⁵ There have also been several exciting developments that can push even beyond this (22,22) active space size through various means of reducing the number of determinants that are included in the CAS wavefunction, including the Selected CI approach using a basis of tensor product states,⁶⁶ adaptive sampling CI,⁶⁷ the so-called iCISCF approach,⁶⁸ and active learning approaches to CI.⁶⁹ Additionally, a family of active-space approaches where the 2-particle reduced density matrix (rather than the many-electron wavefunction) is variationally optimized can also enable active spaces beyond this (22,22) limit,^{70–73} including CASSCF-like calculations with active spaces as large as (64,64).⁷⁴ In this work, we adopt a serial implementation of the direct CI approach of Olsen and co-workers to *ab initio* QED using the Pauli–Fierz Hamiltonian within the dipole and Born–Oppenheimer approximation. We present two formulations of QED-CASCI: PN-QED-CASCI, in which the photonic space is represented in the basis of photon number (PN) states, and CS-QED-CASCI, in which the photonic space is represented in the coherent state (CS) basis. Our serial implementation can routinely handle (12,12) active spaces for the electronic subsystem with at least 100 photonic states.

Theory

We will discuss QED-CASCI as an approach to the energy eigenstates of the Pauli–Fierz (PF) Hamiltonian^{32,33,75–77} within the Born–Oppenheimer and dipole approximations. The Pauli–Fierz

Hamiltonian for a molecular system coupled to a single photonic mode in atomic units as

$$\hat{H}_{\text{PF}} = \hat{H}_e + \omega \hat{b}^\dagger \hat{b} - \sqrt{\frac{\omega}{2}} \boldsymbol{\lambda} \cdot \hat{\boldsymbol{\mu}} (\hat{b}^\dagger + \hat{b}) + \frac{1}{2} (\boldsymbol{\lambda} \cdot \hat{\boldsymbol{\mu}})^2 \quad (1)$$

Here, \hat{H}_e is the standard molecular electronic Hamiltonian within the Born–Oppenheimer approximation, ω is the cavity photon frequency, $\hat{\boldsymbol{\mu}}$ is the molecular dipole operator, $\boldsymbol{\lambda}$ is a coupling vector, and \hat{b}^\dagger , \hat{b} are creation and annihilation operators for the cavity photonic mode, respectively. The coupling vector can be written in terms of the cavity volume, $\boldsymbol{\lambda} = \sqrt{\frac{\hbar}{\epsilon_0 V}} \hat{\mathbf{e}}$. The light-matter coupling in the Pauli–Fierz Hamiltonian may also be written in terms of the vector potential operator $\mathbf{A}_0 (\hat{b}^\dagger + \hat{b})$; for readers familiar with this notation, we note that $\mathbf{A}_0 = \sqrt{\frac{\hbar}{2\omega\epsilon_0 V}} \hat{\mathbf{e}}$, we can write $\mathbf{A}_0 = \sqrt{\frac{1}{2\omega}} \boldsymbol{\lambda}$.^{30,33} Here, we have limited our considerations to a single cavity mode, but the above Hamiltonian is easily generalized for multiple modes (which leads to increased dimensionality) as discussed in prior work.^{55,58} The second term $\hat{H}_{\text{cav}} = \omega \hat{b}^\dagger \hat{b}$ represents the Hamiltonian for the bare cavity mode, which is a harmonic oscillator with fundamental frequency ω . The last two terms are the bilinear coupling, $\hat{H}_{\text{blc}} = -\sqrt{\frac{\omega}{2}} (\boldsymbol{\lambda} \cdot \hat{\boldsymbol{\mu}}) (\hat{b}^\dagger + \hat{b})$, and dipole self-energy terms $\hat{H}_{\text{dse}} = \frac{1}{2} (\boldsymbol{\lambda} \cdot \hat{\boldsymbol{\mu}})^2$, respectively. We will assume a Cartesian coordinate system where $\boldsymbol{\lambda}$ and $\hat{\boldsymbol{\mu}}$ will have x , y , and z components. The molecular dipole operator $\hat{\boldsymbol{\mu}}$ has both electronic and a nuclear contributions, *i.e.*, $\hat{\boldsymbol{\mu}} = \hat{\boldsymbol{\mu}}_e + \boldsymbol{\mu}_n$. In the Born–Oppenheimer approximation, the nuclear contribution is a constant for a given geometry. In the remainder of the paper, we will adopt the notation $\hat{d} = \boldsymbol{\lambda} \cdot \hat{\boldsymbol{\mu}}$ for simplicity, and in cases where we require only the electronic part of this operator, we will denote it as \hat{d}_e and we will denote the nuclear contribution as d_n .

The formulation of mean-field theories of Eq. 1 (e.g. QED–Hartree–Fock, QED–HF) is aided by transformation to the coherent-state basis,^{33,78}

$$\hat{H}_{\text{CS}} = \hat{U}_{\text{CS}} \hat{H}_{\text{PF}} \hat{U}_{\text{CS}}^\dagger. \quad (2)$$

This coherent-state transformation is defined as

$$\hat{U}_{\text{CS}} = \exp\left(z(\hat{b}^\dagger - \hat{b})\right) \quad (3)$$

where z is a parameter defined such that $\langle \Phi_0^e | \hat{U}_{\text{CS}} (\hat{H}_{\text{cav}} + \hat{H}_{\text{blc}} + \hat{H}_{\text{dse}}) \hat{U}_{\text{CS}}^\dagger | \Phi_0^e \rangle$ is a diagonal operator, where $|\Phi_0^e\rangle$ denotes the electronic reference determinant. In particular, this holds when

$$z = \frac{-\langle \hat{d} \rangle}{\sqrt{2\omega}}. \quad (4)$$

The term $\langle \hat{d} \rangle = \boldsymbol{\lambda} \cdot \langle \hat{\boldsymbol{\mu}} \rangle$ in Eq. 4 is computed from the expectation value of the molecular dipole moment which typically comes from a modified Hartree–Fock calculation that includes cavity effects, e.g. QED-HF.^{55,78} Applying this transformation with this choice of z to Eq. 1 yields the Pauli–Fierz Hamiltonian in the coherent state basis:

$$\hat{H}_{\text{CS}} = \hat{H}_e + \omega \hat{b}^\dagger \hat{b} - \sqrt{\frac{\omega}{2}} [\hat{d}_e - \langle \hat{d}_e \rangle] (\hat{b}^\dagger + \hat{b}) + \frac{1}{2} [\hat{d}_e - \langle \hat{d}_e \rangle]^2. \quad (5)$$

We will formulate QED-CASCI for both Eq. 1 and Eq. 5, which we will denote PN-QED-CASCI and CS-QED-CASCI to make reference to the photon number (PN) basis and coherent state (CS) basis for the photonic degrees of freedom, respectively. Although we will consider the reference states to be $|R\rangle = |\Phi_0^e\rangle \otimes |0^P\rangle$ in both cases, we note there are two key differences between these formulations. The first difference between these formulations is that the reference for CS-QED-CASCI formally includes an infinite number of photon occupation states through

$$\hat{U}_{\text{CS}}^\dagger |0^P\rangle = \sum_n c_n (\hat{b}^\dagger)^n |0^P\rangle, \quad (6)$$

where the right hand side of Eq. 6 defines a coherent state wavefunction for a photon.^{30,33,77,78}

The second difference is that the electronic reference determinant is written in terms of canonical molecular orbitals for the PN-QED-CASCI formulation and in terms of QED-HF orbitals in the

CS-QED-CASCI formulations. This latter difference represents a particular choice of a single-electron orbital basis; there are many other valid choices of this orbital basis³⁴ that can be explored in future work. One implication of this choice, however, is that the orbital basis of CS-QED-CASCI depends on the details of the cavity, while the orbital basis of PN-QED-CASCI does not.

A general correlated wave function for a many-electron system coupled to a single-mode cavity can take the form

$$|\Psi\rangle = \sum_n \sum_I C_{I,n} |\Phi_I^e\rangle \otimes |n^p\rangle \quad (7)$$

where $|\Phi_I^e\rangle$ represents a determinant of electronic orbitals, $|n^p\rangle$ is a photon-number state corresponding to n photons in the cavity mode, and $C_{I,n}$ is an expansion coefficient. In the CASCI ansatz for the electronic subspace, a subset of active electrons and orbitals are identified where a full CI expansion is performed within that active space. We use the convention $(N_{\text{el}}, N_{\text{orb}})$ to denote an active space consisting N_{orb} active orbitals including the m highest-energy occupied orbitals containing N_{el} active electrons and the $(N_{\text{orb}} - m)$ remaining lowest-energy unoccupied orbitals. A schematic of one possible determinant in a (6,6) active space is shown in Figure 1. As previously

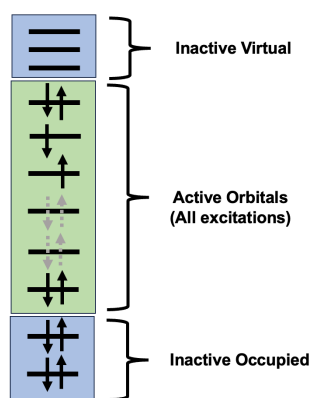


Figure 1: Schematic of the electronic contribution to the QED-CASCI wavefunction.

discussed, because we perform an FCI expansion within the active space, the number of electronic determinants N_{det} in Eq. 7 scales factorially with the number of active electrons and orbitals. However, N_{det} is insensitive to the total size of the single-electron orbital basis used for a given active space size. We can then see that the key to having a tractable CASCI (and QED-CASCI) method relies on having a reasonably sized active space. We also have additional scaling of the number of

electronic-photonic product states in Eq. 7 by maximum photon occupation. For example, if we restrict the maximum photon occupation state to be 1 (so that the photon basis states include $|0^P\rangle$ and $|1^P\rangle$), then we will have twice as many configurations in Eq. 7 as compared to a cavity-free calculation with the same active space and the resulting Hamiltonian matrix will be four times as large. In general, the size of the QED-CASCI wavefunction grows as $(N^P + 1)N_{\text{det}}$ where N^P denotes the maximum photon occupation state. We will use the nomenclature PN-QED-CASCI($N_{\text{el}}, N_{\text{orb}}$)- N^P / CS-QED-CASCI($N_{\text{el}}, N_{\text{orb}}$)- N^P to denote the electronic active space and photonic space truncation in the photon number and coherent state formulations of QED-CASCI, respectively.

The variational QED-CASCI problem in the photon number or coherent state representation formally involves building and diagonalizing the matrix representation of Eq. 1 or Eq. 5, respectively, in the basis of states shown in Eq. 7. The CI matrix in both representations with a maximum photon occupation of N^P will read:

$$\mathbf{H} = \begin{bmatrix} \mathbf{A} + \Delta & \mathbf{G} & 0 & \dots & 0 & 0 \\ \mathbf{G} & \mathbf{A} + \Delta + \Omega & \sqrt{2}\mathbf{G} & \dots & 0 & 0 \\ 0 & \sqrt{2}\mathbf{G} & \mathbf{A} + \Delta + 2\Omega & \dots & 0 & 0 \\ \vdots & \vdots & \vdots & \ddots & \vdots & \vdots \\ 0 & 0 & 0 & \dots & \mathbf{A} + \Delta + (N^P - 1)\Omega & \sqrt{N^P}\mathbf{G} \\ 0 & 0 & 0 & \dots & \sqrt{N^P}\mathbf{G} & \mathbf{A} + \Delta + N^P\Omega \end{bmatrix}. \quad (8)$$

Here the matrix elements of \mathbf{A} are

$$\begin{aligned} A_{In,Jm} &= \langle n^P | \langle \Phi_I^e | \hat{H}_e | \Phi_J^e \rangle | m^P \rangle \\ &= \langle \Phi_I^e | \hat{H}_e | \Phi_J^e \rangle \delta_{nm}, \end{aligned} \quad (9)$$

which are common integrals in CI calculations. For PN-QED-CASCI, these and all subsequent integrals are performed in the canonical MO basis, whereas for CS-QED-CASCI, we transform these and all subsequent integrals to the (orthonormal) QED-HF basis. The elements of Δ and \mathbf{G}

involve slightly different integrals for the photon number formulation as compared to the coherent state formulation. The matrix elements of Δ in the photon number formulation are

$$\begin{aligned}\Delta_{In,Jm} &= \langle n^P | \langle \Phi_I^e | \hat{H}_{\text{dse}} | \Phi_J^e \rangle | m^P \rangle \\ &= \langle \Phi_I^e | \hat{H}_{\text{dse}} | \Phi_J^e \rangle \delta_{nm} \\ &= \frac{1}{2} (\langle \Phi_I^e | \hat{d}_e^2 | \Phi_J^e \rangle + 2d_n \langle \Phi_I^e | \hat{d}_e | \Phi_J^e \rangle + d_n^2 \delta_{IJ}) \delta_{nm},\end{aligned}\quad (10)$$

and for the coherent state formulation are

$$\begin{aligned}\Delta_{In,Jm} &= \langle n^P | \langle \Phi_I^e | \hat{H}_{\text{dse}} | \Phi_J^e \rangle | m^P \rangle \\ &= \langle \Phi_I^e | \hat{H}_{\text{dse}} | \Phi_J^e \rangle \delta_{nm} \\ &= \frac{1}{2} (\langle \Phi_I^e | \hat{d}_e^2 | \Phi_J^e \rangle - 2\langle \hat{d}_e \rangle \langle \Phi_I^e | \hat{d}_e | \Phi_J^e \rangle + \langle \hat{d}_e \rangle^2 \delta_{IJ}) \delta_{nm}.\end{aligned}\quad (11)$$

The elements of \mathbf{G} are

$$\begin{aligned}G_{In,Jm} &= \langle n^P | \langle \Phi_I^e | \hat{H}_{\text{blc}} | \Phi_J^e \rangle | m^P \rangle \\ &= \langle \Phi_I^e | \hat{H}_{\text{blc}} | \Phi_J^e \rangle (\sqrt{m+1} \delta_{n,m+1} + \sqrt{m} \delta_{n,m-1})\end{aligned}\quad (12)$$

where in the photon number formulation,

$$\langle \Phi_I^e | \hat{H}_{\text{blc}} | \Phi_J^e \rangle = -\sqrt{\frac{\omega}{2}} (\langle \Phi_I^e | \hat{d}_e | \Phi_J^e \rangle + d_n \delta_{IJ}). \quad (13)$$

and in the coherent state formulation,

$$\langle \Phi_I^e | \hat{H}_{\text{blc}} | \Phi_J^e \rangle = -\sqrt{\frac{\omega}{2}} (\langle \Phi_I^e | \hat{d}_e | \Phi_J^e \rangle - \langle \hat{d}_e \rangle \delta_{IJ}). \quad (14)$$

Finally, the elements of Ω for both formulations are given by

$$\Omega_{In,Jm} = \langle n^P | \langle \Phi_I^e | \hat{H}_{\text{cav}} | \Phi_J^e \rangle | m^P \rangle = m\omega \delta_{IJ} \delta_{nm}. \quad (15)$$

The block structure shown in Eq. 8 reflects the Kronecker deltas in the expressions for the matrix elements. Each of these integrals over many-electron determinants can be simplified using the Slater–Condon rules⁷⁹ and expressed in terms of 1- and 2-electron integrals in the canonical MO basis for the PN-QED-CASCI formulation or in the QED-HF MO basis for the CS-QED-CASCI formulation; we make use of these expressions in the subsequent section on the Implementation Details.

Implementation Details

For most CI problems, it is not practical to build and store the Hamiltonian matrix. Rather, one typically employs so-called direct CI schemes that employ an iterative eigensolver for one or a few states where the requisite Hamiltonian matrix elements are computed on the fly.^{63,64} Here, we outline the adaptation of such a direct approach to the QED-CASCI problem specifically for the Hamiltonian in the coherent state basis (Eq. 5); as noted in Equations 10-14, one can follow the details with a few key substitutions in the integrals to obtain the implementation for the photon number basis (Eq. 1).

The Hamiltonian in Equation 5 can be rewritten as:

$$\hat{H}_{CS} = \hat{H}'_e + \omega b^\dagger b - \sqrt{\frac{\omega}{2}} (d_{pq} \hat{E}_{pq} - \langle \hat{d}_e \rangle) (b^\dagger + b) + \frac{1}{2} \langle \hat{d}_e \rangle^2 \quad (16)$$

where \hat{E}_{pq} is a generator of the unitary group:

$$\hat{E}_{pq} = \hat{E}_{pq}^\alpha + \hat{E}_{pq}^\beta = \hat{a}_{p\alpha}^\dagger \hat{a}_{q\alpha} + \hat{a}_{p\beta}^\dagger \hat{a}_{q\beta}, \quad (17)$$

The alpha and beta parts of the generator are represented by \hat{E}_{pq}^α and \hat{E}_{pq}^β , respectively. The modified electronic Hamiltonian is given by:

$$\hat{H}'_e = \left(h_{pq} - \frac{1}{2} q_{pq} - \langle \hat{d}_e \rangle d_{pq} \right) \hat{E}_{pq} + \frac{1}{2} ((pq|rs) + d_{pq} d_{rs}) (\hat{E}_{pq} \hat{E}_{rs} - \delta_{qr} \hat{E}_{ps}). \quad (18)$$

The terms h_{pq} and $(pq|rs)$ denote the standard 1- and 2-electron integrals over spatial orbitals in Chemist's notation, d_{pq} and q_{pq} represent modified electric dipole and electric quadrupole integrals, which are given by:

$$d_{pq} = - \sum_{a \in \{x,y,z\}} \lambda_a \int \phi_p^*(\mathbf{r}) r_a \phi_q(\mathbf{r}) d\mathbf{r} \quad (19)$$

$$q_{pq} = - \sum_{ab \in \{x,y,z\}} \lambda_a \lambda_b \int \phi_p^*(\mathbf{r}) r_a r_b \phi_q(\mathbf{r}) d\mathbf{r}. \quad (20)$$

Here, λ_a is a cartesian component of $\boldsymbol{\lambda}$, and r_a is a Cartesian component of the electronic position operator [*e.g.*, for $\mathbf{r} = (x, y, z)$, $r_x = x$]. Next, we define the modified 1- and 2-electron integrals as follows:

$$h'_{pq} = h_{pq} - \frac{1}{2} q_{pq} - \langle \hat{d}_e \rangle d_{pq} \quad (21)$$

$$(pq|rs)' = (pq|rs) + d_{pq} d_{rs}. \quad (22)$$

The eigenvalues of the Hamiltonian 16 in a CI space are obtained from an iterative process using Davidson algorithm,⁸⁰ where the most time-consuming step at each iteration is to compute

the σ vector:

$$\begin{aligned}
 \sigma_{I,m} &= \langle \Phi_I^e, m^p | \hat{H}_{CS} | \Phi_J^e, n^p \rangle C_{J,n} & (23) \\
 &= h'_{pq} \langle \Phi_I^e | \hat{E}_{pq} | \Phi_J^e \rangle C_{J,m} + \frac{1}{2} (pq|rs)' \langle \Phi_I^e | (\hat{E}_{pq} \hat{E}_{rs} - \delta_{qr} \hat{E}_{ps}) | \Phi_J^e \rangle C_{J,m} \\
 &\quad - \sqrt{\frac{\omega}{2}} d_{pq} \langle \Phi_I^e | \hat{E}_{pq} | \Phi_J^e \rangle (\sqrt{m} C_{J,m-1} + \sqrt{m+1} C_{J,m+1}) \\
 &\quad + \sqrt{\frac{\omega}{2}} \langle \hat{d}_e \rangle (\sqrt{m} C_{I,m-1} + \sqrt{m+1} C_{I,m+1}) \\
 &\quad + (m\omega + \frac{1}{2} \langle \hat{d}_e \rangle^2) C_{I,m} & (24)
 \end{aligned}$$

Following Handy⁸¹ we express a Slater determinant as a combination of an alpha string and a beta string:

$$|I\rangle = \alpha(I_\alpha) \beta(I_\beta) |vac\rangle \quad (25)$$

where an alpha/beta string is an ordered product of creation operators for alpha/beta molecular spin orbitals. Applying the Olsen method,⁸² σ is rewritten as:

$$\sigma = (\sigma_e)_1 + (\sigma_e)_2 + (\sigma_e)_3 + (\sigma_{blc})_1 + (\sigma_{blc})_2 + \sigma_{const} \quad (26)$$

where

$$\begin{aligned}
 (\sigma_e)_1(I_\alpha, I_\beta, m) &= \langle \beta(I_\beta) | \hat{E}_{pq}^\beta | \beta(J_\beta) \rangle (h'_{pq} - \frac{1}{2}(pr|rq)') C(I_\alpha, J_\beta, m) \\
 &+ \frac{1}{2} \langle \beta(I_\beta) | \hat{E}_{pq}^\beta \hat{E}_{rs}^\beta | \beta(J_\beta) \rangle (pq|rs)' C(I_\alpha, J_\beta, m)
 \end{aligned} \tag{27}$$

$$\begin{aligned}
 (\sigma_e)_2(I_\alpha, I_\beta, m) &= \langle \alpha(I_\alpha) | \hat{E}_{pq}^\alpha | \alpha(J_\alpha) \rangle (h'_{pq} - \frac{1}{2}(pr|rq)') C(J_\alpha, I_\beta, m) \\
 &+ \frac{1}{2} \langle \alpha(I_\alpha) | \hat{E}_{pq}^\alpha \hat{E}_{rs}^\alpha | \alpha(J_\alpha) \rangle (pq|rs)' C(J_\alpha, I_\beta, m)
 \end{aligned} \tag{28}$$

$$(\sigma_e)_3(I_\alpha, I_\beta, m) = \langle \beta(I_\beta) | \hat{E}_{pq}^\beta | \beta(J_\beta) \rangle \langle \alpha(I_\alpha) | \hat{E}_{rs}^\alpha | \alpha(J_\alpha) \rangle (pq|rs)' C(J_\alpha, J_\beta, m) \tag{29}$$

$$\begin{aligned}
 (\sigma_{blc})_1(I_\alpha, I_\beta, m) &= -\sqrt{\frac{\omega}{2}} d_{pq} \langle \beta(I_\beta) | \hat{E}_{pq}^\beta | \beta(J_\beta) \rangle \\
 &\times (\sqrt{m} C(I_\alpha, J_\beta, m-1) + \sqrt{m+1} C(I_\alpha, J_\beta, m+1))
 \end{aligned} \tag{30}$$

$$\begin{aligned}
 (\sigma_{blc})_2(I_\alpha, I_\beta, m) &= -\sqrt{\frac{\omega}{2}} d_{pq} \langle \alpha(I_\alpha) | \hat{E}_{pq}^\alpha | \alpha(J_\alpha) \rangle \\
 &\times (\sqrt{m} C(J_\alpha, I_\beta, m-1) + \sqrt{m+1} C(J_\alpha, I_\beta, m+1))
 \end{aligned} \tag{31}$$

$$\begin{aligned}
 (\sigma_{const})(I_\alpha, I_\beta, m) &= \sqrt{\frac{\omega}{2}} \langle \hat{d}_e \rangle (\sqrt{m} C(I_\alpha, I_\beta, m-1) + \sqrt{m+1} C(I_\alpha, I_\beta, m+1)) \\
 &+ (m\omega + \frac{1}{2} \langle \hat{d}_e \rangle^2) C(I_\alpha, I_\beta, m)
 \end{aligned} \tag{32}$$

We have adapted the algorithm to evaluate the first two terms from Ref. 82. The sigma vector corresponding to bilinear coupling terms can be calculated in a similar fashion to the one-electron part of $(\sigma_e)_1$ and $(\sigma_e)_2$. The last term is simply a product of scalars and the CI vector. The construction of σ_3 is the most time-consuming step in the Olsen method. We use the algorithm for building σ_3 described in Ref. 83 by rewriting Eqn.29 as follows:

$$\begin{aligned}
 \sigma_3(I_\alpha, I_\beta, m) &= \langle \alpha(I_\alpha) | \hat{E}_{ii}^\alpha | \alpha(I_\alpha) \rangle \langle \beta(I_\beta) | \hat{E}_{jj}^\beta | \beta(I_\beta) \rangle (ii|jj)' C(I_\alpha, I_\beta, m) \\
 &+ \langle \alpha(I_\alpha) | \hat{E}_{ii}^\alpha | \alpha(I_\alpha) \rangle \langle \beta(I_\beta) | \hat{E}_{iu}^\beta | \beta(J_\beta) \rangle (ii|tu)' C(I_\alpha, J_\beta, m) \\
 &+ \langle \alpha(I_\alpha) | \hat{E}_{iu}^\alpha | \alpha(J_\alpha) \rangle \langle \beta(I_\beta) | \hat{E}_{ii}^\beta | \beta(I_\beta) \rangle (tu|ii)' C(J_\alpha, I_\beta, m) \\
 &+ \langle \alpha(I_\alpha) | \hat{E}_{iu}^\alpha | \alpha(J_\alpha) \rangle \langle \beta(I_\beta) | \hat{E}_{vw}^\beta | \beta(J_\beta) \rangle (tu|vw)' C(J_\alpha, J_\beta, m)
 \end{aligned} \tag{33}$$

where the indices i, j represent inactive orbitals and indices t, u, v, w represent active orbitals. As the first three terms of this equation can be built trivially, we now focus on the last term. First, a resolution of identity is inserted into the last term of this equation to give:

$$\begin{aligned} & \langle \alpha(I_\alpha) | \hat{E}_{tu}^\alpha | \alpha(J_\alpha) \rangle \langle \beta(I_\beta) | \hat{E}_{vw}^\beta | \beta(J_\beta) \rangle (tu|vw)' C(J_\alpha, J_\beta, m) \\ &= \langle \alpha(I_\alpha) | \hat{a}_{t\alpha}^\dagger | \alpha(K_\alpha) \rangle \langle \alpha(K_\alpha) | \hat{a}_{u\alpha} | \alpha(J_\alpha) \rangle \langle \beta(I_\beta) | \hat{E}_{vw}^\beta | \beta(J_\beta) \rangle (tu|vw)' C(J_\alpha, J_\beta, m) \end{aligned} \quad (34)$$

The strings $|\alpha(K_\alpha)\rangle$ has one electron less than the reference state. Then the construction of σ_3 (for the active part) becomes a sequence of three operations:

$$D(K_\alpha, u, J_\beta, m) = \langle \alpha(K_\alpha) | \hat{a}_{u\alpha} | \alpha(J_\alpha) \rangle C(J_\alpha, J_\beta, m) \quad (35)$$

$$T(K_\alpha, t, I_\beta, m) = \langle \beta(I_\beta) | \hat{E}_{vw}^\beta | \beta(J_\beta) \rangle (tu|vw)' D(K_\alpha, u, J_\beta, m) \quad (36)$$

$$\sigma_3(I_\alpha, I_\beta, m) = \sigma_3(I_\alpha, I_\beta, m) + \langle \alpha(I_\alpha) | \hat{a}_{t\alpha}^\dagger | \alpha(K_\alpha) \rangle T(K_\alpha, t, I_\beta, m) \quad (37)$$

Among these steps, the inner loop of Eq. 36 can be evaluated as matrix-matrix multiplication.

The Davidson algorithm requires exact or approximate diagonal elements of the Hamiltonian matrix. In our work, we adapt the exact formulation of determinant energy in Ref. 84 with additional terms belonging to the PF Hamiltonian. The expression for the energy of each determinant reads:

$$\begin{aligned} d_{I,m} &= \langle \Phi_I^e, m^p | \hat{H}_{CS} | \Phi_I^e, m^p \rangle \\ &= \sum_i n_i (i|h|i)' + \frac{1}{2} \sum_{ij} n_i n_j (ii|jj)' - \frac{1}{2} (n_i^\alpha n_j^\alpha + n_i^\beta n_j^\beta) (ij|ji)' \\ &\quad + m\omega + \frac{1}{2} \langle \hat{d}_e \rangle^2 \end{aligned} \quad (38)$$

where $n_i^\alpha = 0$ or 1 is the occupation number of alpha spin in spatial orbital ϕ_i , $n_i = n_i^\alpha + n_i^\beta$ is the total occupation number of spatial orbital ϕ_i .

Results and Discussion

We consider several model closed-shell systems for which we can establish an exact benchmark using QED-FCI with a saturated photon basis, including LiH in a 6-311G basis set, H_2O^{2+} cation and BH_3 in a 6-31G basis set. This selection of model systems includes a non-polar (but polarizable) molecule (BH_3), a polar molecule (LiH), and a molecule with net charge (H_2O^{2+}), which engenders a range of coupling behavior between the molecule and the photon field. After analyzing the behavior of both formulations of QED-CASCI for these three systems with respect to an exact benchmark, we conclude with an illustrative calculation of the naphthalene molecule treated in the cc-pVDZ basis set. Here, we explore the behavior of singlet polariton states for a range of coupling strengths leading to inversion of a singlet-triplet ordering in a (12,12) active space, and also illustrate the scaling of our approach with respect to the number of photon states within this active space.

Although we have remarked that the reference determinant in the coherent state basis includes an infinite number of photonic states by virtue of Eq. 6, this does not automatically guarantee that the photon basis for the subsequent QED-CASCI problem is complete. One reason for this is that the specific form of the coherent state transformation (i.e., the value of z in Eq. 3) is derived self-consistently from the QED-HF procedure, which is variationally optimized for the direct product of the coherent state wavefunction for the photon and a single Slater determinant for the electrons. Therefore, we can imagine that there exists a different coherent state transformation for a given electronic state represented as a QED-CASCI or QED-FCI expansion. Nevertheless, we will show that the coherent state formulation may provide a more rapidly converging photon basis for QED-CASCI approaches.

LiH

To illustrate the convergence behavior of the photon basis, we first consider doing PN-QED-FCI and CS-QED-FCI on the bond stretch of the LiH diatomic molecule in a 6-311G basis. We consider

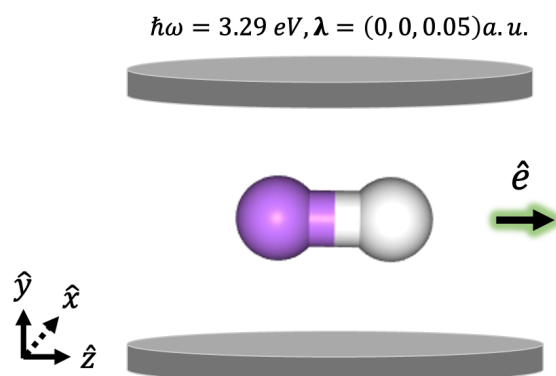


Figure 2: Schematic of LiH system coupled to a cavity mode with $\lambda = (0, 0, 0.05)$ a.u., polarized along the internuclear axis, and $\hbar\omega = 3.29$ eV.

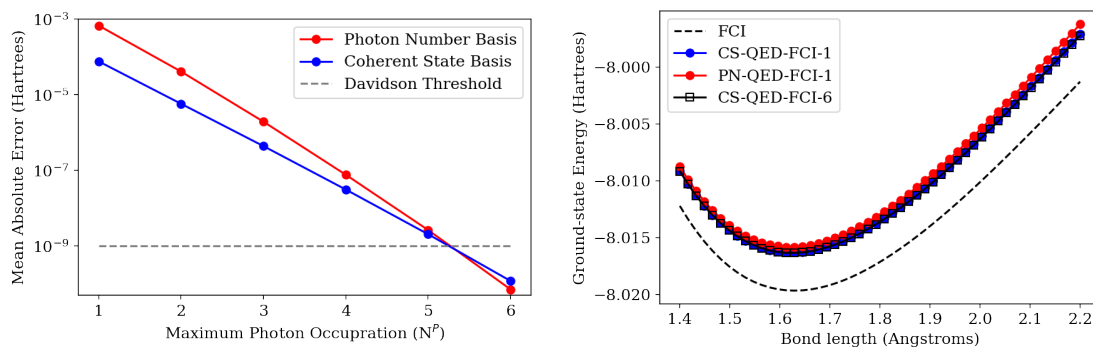


Figure 3: (Left) Mean Absolute Error across the ground-state potential energy scan of LiH coupled to a photon with $\lambda = (0, 0, 0.05)$ a.u. and $\hbar\omega = 3.29$ eV as a function of the size of the photon basis in the photon number and coherent state representations. The reference energies come from CS-QED-FCI-10/6-311G; it can be seen that PN-QED-FCI-6 and CS-QED-FCI-6 are both fully photon-converged. (Right) The ground-state potential energy scan of LiH coupled to a photon with $\lambda = (0, 0, 0.05)$ a.u. and $\hbar\omega = 3.29$ eV at the fully photon-converged CS-QED-FCI-6/6-311G level of theory compared to CS-QED-FCI-1/6-311G and PN-QED-FCI-1/6-311G, which represent minimal photon bases in the coherent state and photon number state formulations. The cavity-free FCI/6-311G energy is plotted for reference in the right panel.

this system coupled to a photon with energy tuned to the lowest singlet excitation ($\hbar\omega = 3.29$ eV) and with $\lambda_z = 0.05$ atomic units, polarized along the internuclear axis (see Figure 2). We choose this large value of the field to draw out a clear difference in the convergence behavior of the photon number and coherent state formulations. To explore this convergence behavior, the maximum photon occupation number is systematically increased from $N^P = 1$ to $N^P = 10$, where we could gauge that the photon space is fully converged by $N^P = 6$ since the further increase of N^P does not change the energies of any of the eigenvalues to within the convergence criteria of the Davidson solver ($\approx 10^{-9}$ Hartrees). We examine the mean absolute error of the PES computed using PN-QED-FCI- N^P and CS-QED-FCI- N^P as a function of N^P , and we see that this error is an order of magnitude smaller for the minimal photonic basis in the coherent-state formulation (see Figure 3 right panel). We see that the error decreases approximately linearly as a function of the size of the photonic basis for both formulations, with both approaching the convergence threshold of our Davidson solver by $N^P \approx 6$ (see Figure 3 right panel). We use CS-QED-FCI-10 as the exact benchmark for computation of the mean absolute errors displaced in the left panel of Figure 3. In the right panel of Figure 3, we show the ground-state potential energy stretch of the LiH both outside the cavity (dashed black line) and inside the cavity. For the latter, we compute the PES using PN-QED-FCI-1 and CS-QED-FCI-1 as a minimal photonic basis and CS-QED-FCI-6 as a fully converged photonic basis based on the behavior of the mean absolute error shown in the left panel of Figure 3. We see that all in-cavity PESs are above the cavity-free PES as expected. We also see CS-QED-FCI-6 is a lower bound to both curves in a minimal photonic basis, which follows from the variational nature of these calculations. Consistent with the idea that the coherent state formulation provides a more efficient photonic basis, we can see that the CS-QED-FCI-1 curve lies below the PN-QED-FCI-1 curve and is visually nearly identical to the fully converged result (see Figure 3 right panel).

Next, we consider the lower- and upper-polariton surfaces that emerge in the same LiH system. The left panel of Figure 4 shows the CS-QED-FCI-10/6-311G polariton surfaces (lower-polariton (LP) in red, upper-polariton (UP) in blue) along with the cavity-free FCI/6-311G surfaces for the

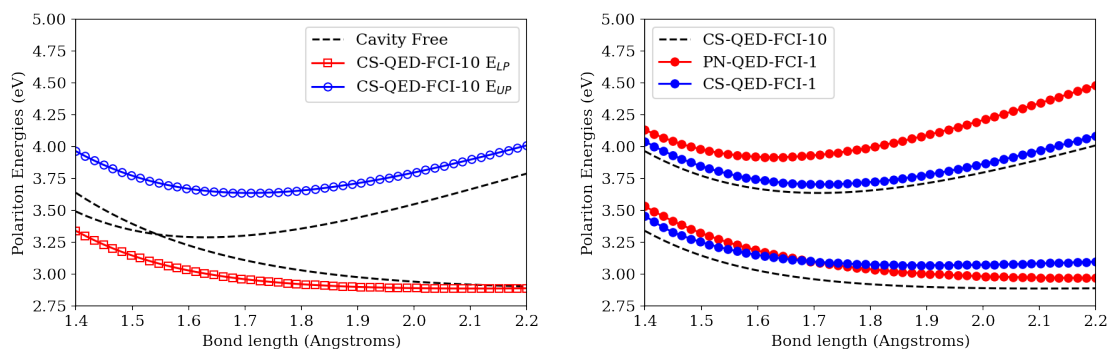


Figure 4: (Left) The polariton potential energy scans of LiH coupled to a photon with $\lambda = (0,0,0.05)$ a.u. and $\hbar\omega = 3.29$ eV at the CS-QED-FCI-10/6-311G level as compared to the cavity-free FCI/6-311G energies of the ground-state surface displaced by $\hbar\omega$ and the first excited singlet state surface. (Right) The polariton potential energy surfaces in the minimal photon basis in the photon number representation (red) and the coherent state representation (blue) compared to the fully-converged polariton potential energy surfaces.

ground-state displaced by the photon energy and the first singlet excited state potential energy surfaces (black dashed lines, see Figure 4 left panel)). The magnitude of the field is evident by the large Rabi splitting between the LP and UP surfaces. We compare the LP and UP surfaces using a minimal photon basis (PN-QED-FCI-1 and CS-QED-FCI-1) to CS-QED-FCI-10 surfaces (see Figure 4 right panel). We can see that the shapes of both polariton surfaces show sensitivity to the size of the photon basis in both the PN and CS formulations. However, the CS-QED-FCI-1 surfaces have greater parallelism with the photon-converged surfaces as compared to the PN-QED-FCI-1 surfaces.

As a final analysis on the LiH system, we investigate the behavior of the ground-state potential energy surface as a function of the active space and photonic basis size for the QED-CASCI method. Specifically, we compute the ground-state potential energy surfaces for the LiH cavity system at the CS-QED-CASCI(4, n)- N^p /6-311G and PN-QED-CASCI(4, n)- N^p /6-311G levels with $n = [3, 15]$ and $N^p = 1$ and 10; note that a (4,16) active space is identical to QED-FCI for LiH in a 6-311G basis set. The non-parallelism errors (NPE) relative to CS-QED-FCI-10/6-311G are shown in Figure 5. Not surprisingly, the PN-QED-CASCI(4, n)-1 surfaces have the highest NPE for all active space sizes, while we observe CS-QED-CASCI(4, n)-10 surfaces having the lowest NPE for all active spaces except the (4,5) active space. Importantly, the CS-QED-CASCI(4, n)-1 NPE are

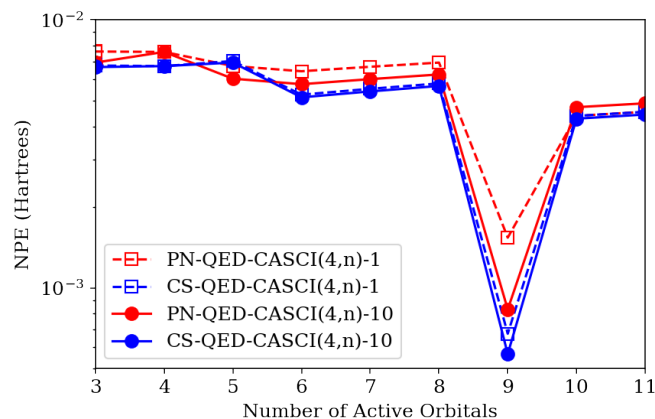


Figure 5: The non-parallelity error (NPE) of the ground-state potential energy surface of LiH coupled to a photon with $\lambda = (0, 0, 0.05)$ a.u. and $\hbar\omega = 3.29$ eV at the QED-CASCI(4, n)- N^p /6-311G level for $n = [3, 11]$ active orbitals and $N^p = 1$ and 10. The NPE is computed relative to CS-QED-FCI-10/6-311G, which is fully photon-converged.

consistently lower than the PN-QED-CASCI(4, n)-10 results for all except the (4,5) active space as well. This suggests that there can be additional sensitivity to the size of the photon basis when the electronic excitation space is truncated that was not evident in the QED-FCI results presented in Figure 3.

H_2O^{2+}

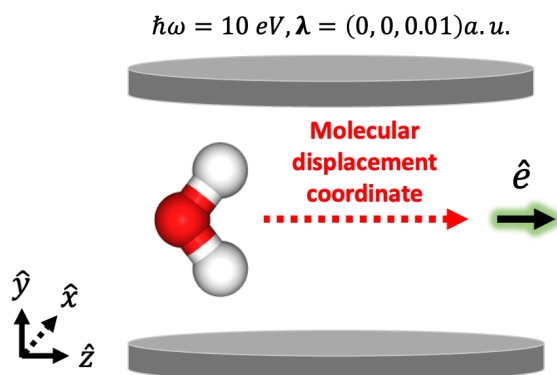


Figure 6: Schematic of H_2O^{2+} system coupled to a cavity mode with $\lambda = (0, 0, 0.01)$ a.u. and $\hbar\omega = 10$ eV where the origin of the molecule is systematically displaced along the polarization direction.

Next, we consider a model charged system, H_2O^{2+} , in the 6-31G basis set coupled to a photon

with $\hbar\omega = 10$ eV with a polarization vector $\lambda = (0, 0, 0.01)$ in atomic units. There are no optically-allowed transitions in the UV-Vis region for this system; the photon energy $\hbar\omega$ is not resonant with any transitions from the FCI/6-31G eigenspectra in this species and is arbitrarily chosen. We keep the geometry fixed at $r_{OH} = 1.0$ Angstroms and $\theta_{HOH} = 104.5^\circ$, which is a typical geometry for neutral water. While this will surely not correspond to an equilibrium geometry for H_2O^{2+} , we simply seek to study the behavior of the QED-CASCI method for a charged closed-shell system for which we can provide a QED-FCI benchmark. Charged molecular species, unlike their neutral counterparts, have origin-dependent dipole moments, which leads to origin-dependent energy errors in certain formulations of *ab initio* QED methods, including QED-HF and QED-CC in the photon number basis.^{33,48}

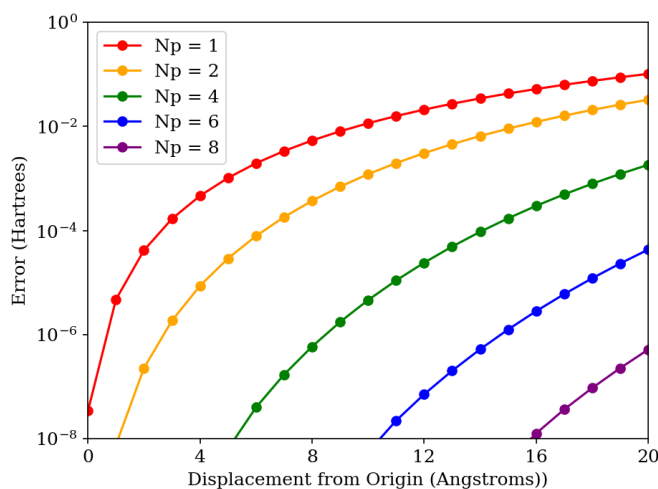


Figure 7: The energy error of the H_2O^{2+} lowest-energy singlet state coupled to a photon with $\lambda = (0, 0, 0.01)$ a.u. and $\hbar\omega = 10$ eV as a function of displacement from the origin for different sizes of the photon basis for the photon number formulation of PN-QED-FCI- N^P /6-31G; here $N^P = 1$ corresponds to the minimal photon basis including the $|0^P\rangle$ and $|1^P\rangle$ occupation states. The reference energies for each displacement come from CS-QED-FCI-1/6-31G, which is origin invariant.

The origin-dependence of QED-HF can be completely alleviated through saturation of the photon basis set or, alternatively, through formulating QED-HF in the coherent-state basis.³³ Similarly, we observe that origin-invariant energies are obtained from the CS-QED-FCI-1 approach. However, the PN-QED-FCI- N^P approach does not generally produce origin-invariant energies for charged species. We examine the energy error in the lowest-energy singlet state of H_2O^{2+} com-

puted by PN-QED-FCI- N^P while displacing the center of mass along the z -axis (see Figure 6, which is the polarization direction of the field and the direction along which dipole moment of H_2O^{2+} is oriented. We see that when $N^P = 1$ (the minimal photon basis, including $|0^P\rangle$ and $|1^P\rangle$ photon number states), the energy approaches the milliHartree range by a displacement of 4 Angstroms from the origin and continues to increase with further displacement (see Figure 7). We also clearly see the mitigating impact that growing the size of the photonic basis has on the origin dependence; for $N^P = 8$, the error is in the microHartree range after a displacement of 20 Angstroms (see Figure 7). We emphasize that since we are performing full CI within the electronic basis, these origin-dependent energy errors are arising solely from truncation of the photonic basis. As we approach the completeness of the photonic basis, we have a fully variational solution within the single electron orbital representation given by the 6-31G basis set, and see that the origin invariance of the energies is properly restored (see Figure 7).

A logical next question is how the QED-CASCI methods perform under truncation of the photonic basis, since here we cannot achieve a fully variational solution even with saturation of the photonic subspace. That is, in QED-CASCI just as in CASCI, the CI coefficients in Eq. 7 are variationally optimized, but the orbital basis is not; this is to be contrasted with approaches like CASSCF/MCSCF, which is fully variational in the sense that the CI coefficients and the orbital basis are variationally optimized.³⁴ We explore this question using three different active spaces: (6,11), (6,9), and (6,6). All active spaces have excluded 2 core electrons and the (6,11) active space excludes the two highest virtual orbitals; i.e., an (8,13) active space is equivalent to FCI for the electronic subspace of this system. We observe that CS-QED-CASCI-1 is nearly origin-independent; in the singlet ground-state energy the subtle origin dependence is negligible compared to the correlation energy that is neglected by truncation of the excitation space (see Figure 8 Top Panel and Table 1). We conjecture this slight origin dependence arises because the specific form of coherent state transformation used (specifically the parameter z in Eq. 3) derives from the QED-HF reference wavefunction and has some error relative to a coherent state transformation that would be derived from a QED-CASCI state. By comparison, the PN-QED-CASCI-1 shows strong origin

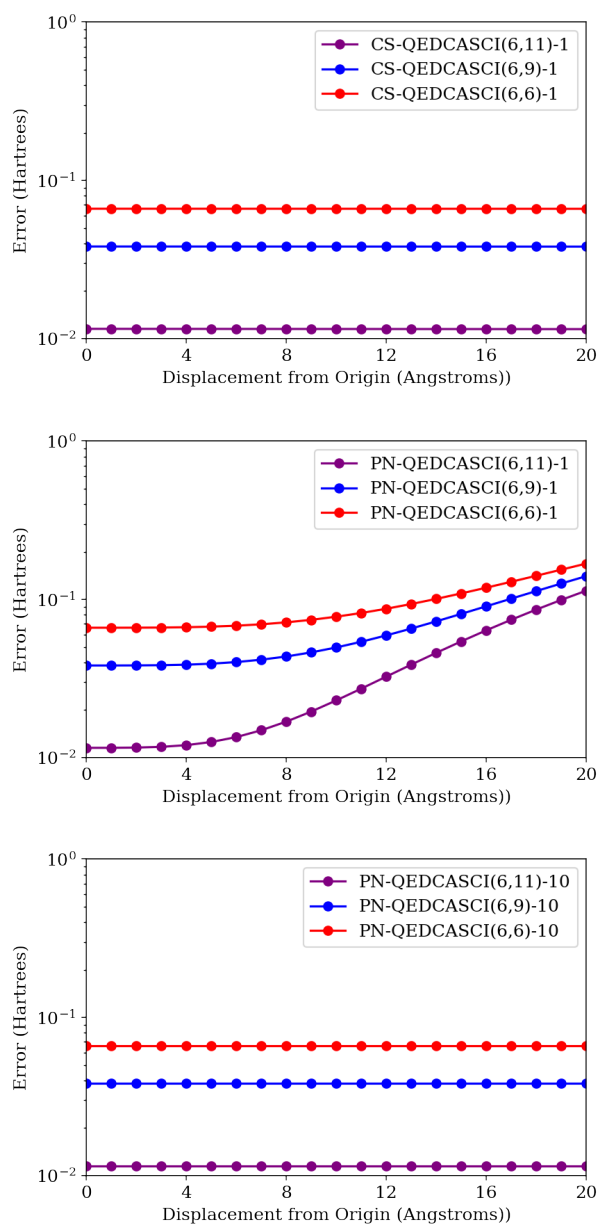


Figure 8: The energy error of the H_2O^{2+} lowest-energy singlet state coupled to a photon with $\lambda = (0, 0, 0.01)$ a.u. and $\hbar\omega = 10$ eV as a function of displacement from the origin for CS-QED-CASCI(6, n)-1 (Top), PN-QED-CASCI(6, n)-1 (Middle), and PN-QED-CASCI(6, n)-10 (Bottom) for $n = 11, 9, 6$ all in a 6-31G basis set. The coherent state formulation shows negligible origin dependence as compared to the correlation error arising from the truncated active space, the photon number formulation shows strong origin dependence when $N^p = 1$ and negligible origin dependence when $N^p = 10$.

dependence that becomes appreciable compared to the correlation error at displacements greater than or equal to 8 Angstroms (see Figure 8 Middle Panel and Table 1). Again, we see that expanding the size of the photon basis to $N^p = 10$ alleviates the origin dependence, giving results that are independent of origin (see Figure 8 Bottom Panel and Table 1).

Table 1: Absolute energy error of the lowest energy singlet state of H_2O^{2+} displaced by 20 Angstroms relative to the origin CS-QED-CASCI(6,n)-1, PN-QED-CASCI(6,n)-1, and PN-QED-CASCI(6,n)-10 levels of theory all in the 6-31G basis set.

Absolute Error at Maximum Displacement (Hartrees)			
	(6,11)	(6,9)	(6,6)
CS $N^p = 1$	$4.90 \cdot 10^{-5}$	$6.62 \cdot 10^{-5}$	$7.62 \cdot 10^{-5}$
PN $N^p = 1$	$1.01 \cdot 10^{-1}$	$1.01 \cdot 10^{-1}$	$1.02 \cdot 10^{-1}$
PN $N^p = 10$	$3.84 \cdot 10^{-9}$	$3.82 \cdot 10^{-9}$	$3.85 \cdot 10^{-9}$

BH₃

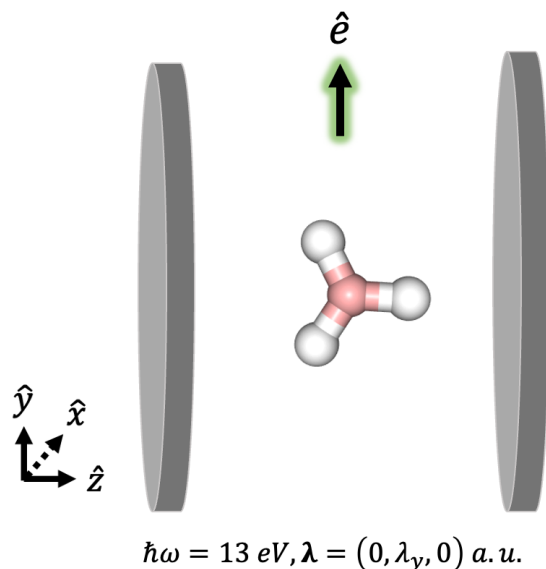


Figure 9: Schematic of BH_3 system coupled to a cavity mode with variable λ polarized along the y -axis and $\hbar\omega = 13 \text{ eV}$.

As a final system with a QED-FCI benchmark, we consider BH_3 within the 6-31G basis set as a non-polar model system. We optimize the geometry of BH_3 the MP2/6-311G level and then

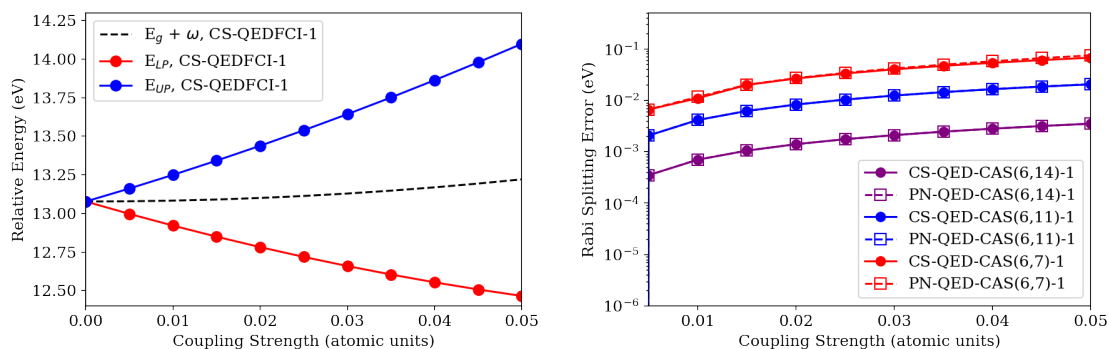


Figure 10: (Left) CS-QED-FCI-1/6-31G in the coherent state basis of BH₃ coupled to a photon with y-polarization tuned to a transition with a strong y-component of the transition dipole moment (3rd singlet excited state); the geometry is optimized at the MP2/6-311G level of theory. Photon energy is 13.07 eV. (Right) Rabi splitting using QED-CASCI(*n,m*)/6-31G in the coherent state basis of BH₃ coupled to a photon with y-polarization tuned to a transition with a strong y-component of the transition dipole moment (3rd singlet excited state); the photon energy is Geometry is optimized at the MP2/6-311G level of theory. Photon energy is 13.65 eV for CASCI(6,7), 13.25 eV for CASCI(6,11), and 13.09 for CASCI(6,14).

find that at FCI/6-31G level, the third singlet excited-state with an excitation energy of 13.07 eV has a strong transition dipole moment oriented along the y-axis in the coordinate system illustrated in Figure 9. We first compute the polariton energies at the CS-QED-FCI-1/6-31G level (see Figure 10) for a range of coupling strengths up to $\lambda_y = 0.05$ a.u. We then computed the polariton energies at the same coupling strengths at the QED-CASCI-1(6,14)/6-31G, QED-CASCI-1(6,11)/6-31G and QED-CASCI-1(6,7)/6-31G in both photon number and coherent state representations. In each case, we used photon energies tuned to the analogous optically-allowed transition at the corresponding CASCI(N_{el}, N_{orb})/6-31G level of theory: $\hbar\omega = 13.65$ eV for CASCI(6,7)/6-31G, $\hbar\omega = 13.25$ eV for CASCI(6,11)/6-31G, and $\hbar\omega = 13.09$ eV for CASCI(6,14)/6-31G. As all of these levels of theory will result in different absolute energies of the polariton states, we compare the Rabi splitting energy (defined as the difference between the upper polariton and lower polariton energies) at each level of theory to the CS-QED-FCI-1/6-31G Rabi splitting for all values of $\lambda_y > 0$ (see Figure 10 right panel); the Rabi splitting goes to 0 by definition with $\lambda_y = 0$. In this system, we see very little difference between the computed Rabi splitting in the photon number and coherent state representations for a given QED-CASCI active space size (see Figure 10 right

panel). However, we do see that the error in the Rabi splitting is rather sensitive to the size of the active space, with the largest (6,14) active space having consistently the smallest error in the Rabi splitting, with errors around 1 meV/36 microHartrees at the strongest coupling strength ($\lambda_y = 0.05$ a.u.). By contrast, the smallest active space (6,7) approaches errors in the Rabi splitting of around 0.1 eV/3.6 mHartree at the strongest coupling strength. The strong dependence of the Rabi splitting error on the active space size suggests that the inclusion of many-body correlation effects along with electron-photon coupling can impact the ability to capture the essential phenomenology of molecular polaritons.

C₈H₁₀

Our final system of study is the naphthalene molecule (C₈H₁₀) coupled to a photon tuned to the transition between the ground-state and the second singlet excited state (⁰S and ²S). This represents the simplest embodiment of the polycyclic aromatic hydrocarbons (PAH) family of molecules that are paradigmatic molecular systems for strong multireference correlation effects.^{70,85–88} Cavity effects in aggregates of PAH systems have also been proposed as a route to enhance singlet fission⁸⁹ and inversion of singlet-triplet gaps.⁹⁰ Here we investigate the ordering of singlet polariton states relative to a nearby triplet state using our CS-QED-CASCI approach. Although we consider only a single molecule coupled to a cavity, we can envision that such calculations may enable the parameterization of accurate models for aggregates to enable future studies. We optimize the geometry at the MP2/cc-pVTZ level of theory using density fitting, and at this geometry, we find the second singlet excited state at both the CASCI(10,10)/cc-pVDZ and CASCI(12,12)/cc-pVDZ level has a transition energy of 5.92 eV and a strong transition dipole moment along the y-axis. The (10,10) active space includes all electrons and orbitals comprising the aromatic system; however, we find that the evolution of the polariton energies becomes non-smooth for values of $\lambda_y > 0.01$ atomic units in this active space, while we observe smooth evolution of the energies for all values of λ_y considered when a (12,12) active space is used.

We track the evolution of the polariton state energies that emerge from coupling the ground-

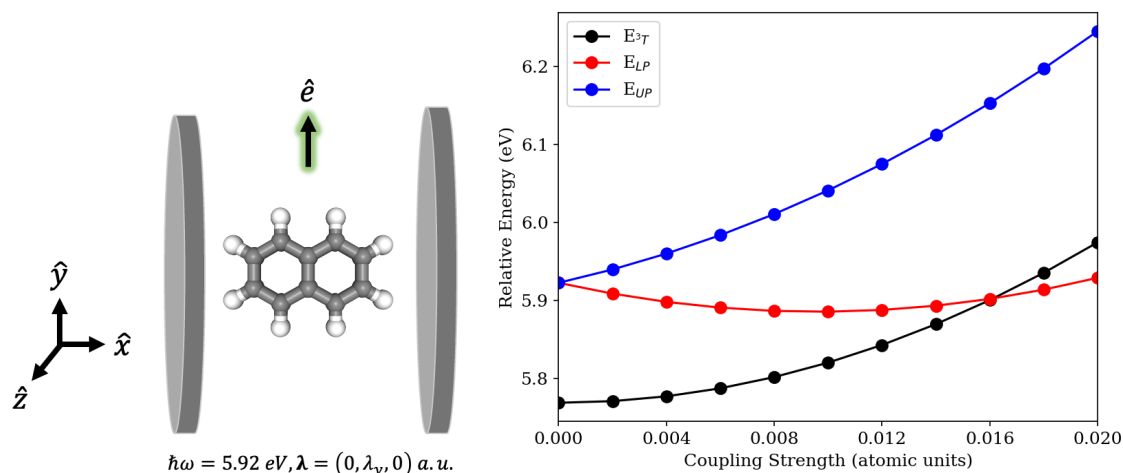


Figure 11: (Left) Schematic of C_8H_{10} system coupled to a cavity mode with variable λ polarized along the y -axis and $\hbar\omega = 5.92 \text{ eV}$. (Right) Relative energies of the polariton states emerging from coupling the ${}^0S \rightarrow {}^2S$ transition to the cavity photon with $\hbar\omega = 5.92 \text{ eV}$ plotted along with the relative energy of a nearby triplet state 3T . The energies are computed relative to the ground-state energy of naphthalene under zero coupling computed at the CASCI(12,12)/cc-pVDZ level.

to-second singlet excited-state (${}^0S \rightarrow {}^2S$) transition along with the energy of a nearby triplet state, which is the third triple excited-state (here denoted 3T). We can see that outside the cavity, the energy of the 2S state lies approximately 0.16 eV above the energy of the 3T state (see Figure 11 right panel under zero coupling). Increasing the coupling strength monotonically increases the upper polariton energy and the energy of the 3T state. While the lower polariton energy initially decreases with increasing coupling strength, we see that it starts to increase for values of $\lambda_y \approx 0.012$ atomic units. Nevertheless, we see that the ordering of the 3T and singlet lower polariton state changes at around $\lambda_y = 0.016$ atomic units. Such an inversion of singlet and triplet states was reported in TADF materials by Kena-Cohen and co-workers⁹⁰ in the collective strong coupling regime. Here we wish to point out a somewhat subtle point of distinction between the behavior of these states in the single molecule coupling regime discussed in this work and the collective coupling regime discussed in Ref. 90. Namely, in the collective coupling regime, the Hamiltonian contribution we call \hat{H}_{blc} would experience a scaling with the number of molecules coupled to a mode, whereas the term \hat{H}_{dse} would not experience this scaling, and this term will affect the Rabi splitting between the singlet polariton states, but will not affect the energetics of the triplet states due to the ab-

sence of a transition dipole moment. However, the increase in the triplet energy we observe arises from the dipole self-energy term (which can couple to the light field through molecular dipole and quadrupole terms), which does not experience number scaling in the collective coupling regime. Hence, the triplet energy is not observably modified under collective strong coupling.⁹⁰

Table 2: Timings of Davidson iterative process for CS-QED-CASCI(12,12)- N^P /cc-pVDZ for different values of N^P . Timings were performed on a Dell Precision 7920 running Ubuntu 22 with a single 3.9 GHz Intel Xeon Gold 6250 processor.

N^P	Number of Determinants	Total size of σ and CI vectors (MB)	Time (s)
1	1707552	1563.4	210.0
2	2561328	2345.0	340.4
4	4268880	3908.2	607.9
10	9391536	8598.2	1429.6
20	17929296	16414.8	2667.9
40	35004816	32047.8	5261.0
80	69155856	63314.1	10366.0
100	86231376	78947.2	12864.9

We also report on the performance of the QED-CASCI method using the naphthalene system. Specifically, we monitor the total number of determinants comprising Eq. 7, the memory size of the σ and CI vectors, and the total time required to converge eigenstates for a series of CS-QED-CASCI(12,12)- N^P /cc-pVDZ calculations. For each calculations, we set $\hbar\omega = 5.92$ eV, $\lambda = (0, 0.01, 0)$ a.u., and solve for the 5 lowest roots of the Hamiltonian. As expected, the number of determinants increases linearly with the size of the photonic basis, specifically as $(N^P + 1) \times N_{\text{det}}^e$ where N_{det}^e is the number of determinants in the electronic subspace that is determined by a given active space size^{63,64} (see Table 2). The size of σ and CI vectors are calculated for the iteration when the maximum size of the subspace is reached during the Davidson iterations; we set the threshold for this maximum value to be 12 for all calculations reported in Table 2, which limits the total size of these vectors to be proportional to $12 \times 5 \times (N_p + 1) \times N_{\text{det}}$, where 5 again comes from the number of roots being solved for. The time to solution tends to be close to linear with the total

number of determinants, with the longest time to solution of < 4 hours seen for the $N^p = 100$ case (see Table 2).

Concluding Remarks

We have developed an approach called QED-CASCI to provide ground- and excited-state polaritonic surfaces with a balanced description of strong correlation effects among electronic and photonic degrees of freedom. This method can provide a platform for ai-CQED when both strong electron correlation and strong light-matter coupling are important and can be leveraged to obtain multiple polaritonic potential energy surfaces and couplings that can be leveraged for *ab initio* molecular dynamics simulations of polariton chemistry. We have implemented two different formulations of QED-CASCI: PN-QED-CASCI which is formulated in the photon-number basis and CS-QED-CASCI which is formulated in the coherent state basis. Both methods were applied to a range of model systems for which we can also provide a numerically exact benchmark using QED-FCI. We have shown that both methods converge to numerically identical answers in the limit that the photon basis becomes complete, but that CS-QED-CASCI shows accelerated convergence that becomes particularly prominent for polar and charged species. The efficiency of our serial implementation was demonstrated on the naphthalene molecule in a (12,12) active space where we can solve for multiple polaritonic states with the inclusion of 100 photonic basis states in roughly 4 hours on a single CPU.

Acknowledgments The authors acknowledge support from the Center for Many-Body Methods, Spectroscopies, and Dynamics for Molecular Polaritonic Systems (MAPOL) under FWP 79715, which is funded as part of the Computational Chemical Sciences (CCS) program by the U.S. Department of Energy, Office of Science, Office of Basic Energy Sciences, Division of Chemical Sciences, Geosciences and Biosciences at Pacific Northwest National Laboratory (PNNL). PNNL is a multi-program national laboratory operated by Battelle Memorial Institute for the

United States Department of Energy under DOE contract number DE-AC05-76RL1830.

Author Declarations The Authors declare no conflict of interest.

Data Availability The implementation of the QED-CASCI method used for the results presented within can be accessed in the following GitHub repository: https://github.com/mapol-chem/qed-ci/tree/jctc_submission.

The data that support the findings of this study are available from the corresponding author upon reasonable request and are openly available in GitHub at https://github.com/FoleyLab/data_repository/tree/jctc_submission/Mapol/.

For LiH data: https://github.com/FoleyLab/data_repository/tree/jctc_submission/Mapol/LiH/

For H₂O²⁺ data: https://github.com/FoleyLab/data_repository/tree/jctc_submission/Mapol/H2O_ions/

For BH₃ data: https://github.com/FoleyLab/data_repository/tree/jctc_submission/Mapol/BH3/

For C₈H₁₀ data: https://github.com/FoleyLab/data_repository/tree/jctc_submission/Mapol/Napthalene/

References

- (1) Lidzey, D. G.; Bradley, D. D. C.; Skolnick, M. S.; Virgili, T.; Walker, S.; Whittaker, D. M. Strong exciton–photon coupling in an organic semiconductor microcavity. *Nature* **1998**, 395, 53–55.
- (2) Bellessa, J.; Bonnard, C.; Plenet, J. C.; Mugnier, J. Strong Coupling between Surface Plasmons and Excitons in an Organic Semiconductor. *Phys. Rev. Lett.* **2004**, 93, 036404.
- (3) Hutchison, J. A.; Schwartz, T.; Genet, C.; Devaux, E.; Ebbesen, T. W. Modifying Chemical Landscapes by Coupling to Vacuum Fields. *Angewandte Chemie International Edition* **2012**, 51, 1592–1596.

- (4) Törmä, P.; Barnes, W. L. Strong coupling between surface plasmon polaritons and emitters: a review. *Reports on Progress in Physics* **2014**, *78*, 013901.
- (5) Coles, D. M.; Yang, Y.; Wang, Y.; Grant, R. T.; Taylor, R. A.; Saikin, S. K.; Aspuru-Guzik, A.; Lidzey, D. G.; Tang, J. K.-H.; Smith, J. M. Strong coupling between chlorosomes of photosynthetic bacteria and a confined optical cavity mode. *Nature Communications* **2014**, *5*, 5561.
- (6) Orgiu, E.; George, J.; Hutchison, J. A.; Devaux, E.; Dayen, J. F.; Doudin, B.; Stellacci, F.; Genet, C.; Schachenmayer, J.; Genes, C.; Pupillo, G.; Samorì, P.; Ebbesen, T. W. Conductivity in organic semiconductors hybridized with the vacuum field. *Nature Materials* **2015**, *14*, 1123–1129.
- (7) Chikkaraddy, R.; de Nijs, B.; Benz, F.; Barrow, S. J.; Scherman, O. A.; Rosta, E.; Demetriadou, A.; Fox, P.; Hess, O.; Baumberg, J. J. Single-molecule strong coupling at room temperature in plasmonic nanocavities. *Nature* **2016**, *535*, 127–130.
- (8) Ebbesen, T. W. Hybrid Light–Matter States in a Molecular and Material Science Perspective. *Accounts of Chemical Research* **2016**, *49*, 2403–2412.
- (9) Sukharev, M.; Nitzan, A. Optics of exciton-plasmon nanomaterials. *Journal of Physics: Condensed Matter* **2017**, *29*, 443003.
- (10) Zhong, X.; Chervy, T.; Zhang, L.; Thomas, A.; George, J.; Genet, C.; Hutchison, J. A.; Ebbesen, T. W. Energy Transfer between Spatially Separated Entangled Molecules. *Angewandte Chemie International Edition* **2017**, *56*, 9034–9038.
- (11) Munkhbat, B.; Wersäll, M.; Baranov, D. G.; Antosiewicz, T. J.; Shegai, T. Suppression of photo-oxidation of organic chromophores by strong coupling to plasmonic nanoantennas. *Science Advances* **2018**, *4*, eaas9552.
- (12) Flick, J.; Rivera, N.; Narang, P. Strong light-matter coupling in quantum chemistry and quantum photonics. *Nanophotonics* **2018**, *7*, 1479 – 1501.

- (13) Frisk Kockum, A.; Miranowicz, A.; De Liberato, S.; Savasta, S.; Nori, F. Ultrastrong coupling between light and matter. *Nature Reviews Physics* **2019**, *1*, 19–40.
- (14) Climent, C.; Galego, J.; Garcia-Vidal, F. J.; Feist, J. Plasmonic Nanocavities Enable Self-Induced Electrostatic Catalysis. *Angewandte Chemie International Edition* **2019**, *58*, 8698–8702.
- (15) Lather, J.; Bhatt, P.; Thomas, A.; Ebbesen, T. W.; George, J. Cavity Catalysis by Cooperative Vibrational Strong Coupling of Reactant and Solvent Molecules. *Angewandte Chemie International Edition* **2019**, *58*, 10635–10638.
- (16) Chevrier, K.; Benoit, J. M.; Symonds, C.; Saikin, S. K.; Yuen-Zhou, J.; Bellessa, J. Anisotropy and Controllable Band Structure in Suprawavelength Polaritonic Metasurfaces. *Phys. Rev. Lett.* **2019**, *122*, 173902.
- (17) Kéna-Cohen, S.; Forrest, S. R. Room-temperature polariton lasing in an organic single-crystal microcavity. *Nature Photonics* **2010**, *4*, 371–375.
- (18) Antoniou, P.; Suchanek, F.; Varner, J. F.; Foley, J. J. Role of Cavity Losses on Nonadiabatic Couplings and Dynamics in Polaritonic Chemistry. *J. Phys. Chem. Lett.* **2020**, *11*, 9063–9069.
- (19) Yadav, R. K.; Otten, M.; Wang, W.; Cortes, C. L.; Gosztola, D. J.; Wiederrecht, G. P.; Gray, S. K.; Odom, T. W.; Basu, J. K. Strongly Coupled Exciton–Surface Lattice Resonances Engineer Long-Range Energy Propagation. *Nano Letters* **2020**, *20*, 5043–5049.
- (20) Hoffmann, N. M.; Lacombe, L.; Rubio, A.; Maitra, N. T. Effect of many modes on self-polarization and photochemical suppression in cavities. *J. Chem. Phys.* **2020**, *153*, 104103.
- (21) Li, T. E.; Subotnik, A. N. J. E. Cavity molecular dynamics simulations of vibrational polariton-enhanced molecular nonlinear absorption. *J. Chem. Phys.* **2021**,
- (22) Brawley, Z. T.; Storm, S. D.; Mora, D. A. C.; Pelton, M.; Sheldon, M. Angle-independent

- plasmonic substrates for multi-mode vibrational strong coupling with molecular thin films. *J. Chem. Phys.* **2021**, *154*, 104305.
- (23) Ishii, T.; Bencheikh, F.; Forget, S.; Chénais, S.; Heinrich, B.; Kreher, D.; Sosa Vargas, L.; Miyata, K.; Onda, K.; Fujihara, T.; Kéna-Cohen, S.; Mathevet, F.; Adachi, C. Enhanced Light–Matter Interaction and Polariton Relaxation by the Control of Molecular Orientation. *Advanced Optical Materials* **2021**, *9*, 2101048.
- (24) Pandya, R.; Ashoka, A.; Georgiou, K.; Sung, J.; Jayaprakash, R.; Renken, S.; Gai, L.; Shen, Z.; Rao, A.; Musser, A. J. Tuning the Coherent Propagation of Organic Exciton-Polaritons through Dark State Delocalization. *Advanced Science* **2022**, *9*, 2105569.
- (25) Hu, W.; Gustin, I.; Krauss, T. D.; Franco, I. Tuning and Enhancing Quantum Coherence Time Scales in Molecules via Light-Matter Hybridization. *J. Phys. Chem. Lett.* **2022**, *13*, 11503–11511, PMID: 36469838.
- (26) Cheng, C.-Y.; Krainova, N.; Brigeman, A. N.; Khanna, A.; Shedge, S.; Isborn, C.; Yuen-Zhou, J.; Giebink, N. C. Molecular polariton electroabsorption. *Nat. Commun.* **2022**, *13*, 7937.
- (27) Li, T. E.; Cui, B.; Subotnik, J. E.; Nitzan, A. Molecular Polaritonics: Chemical Dynamics Under Strong Light–Matter Coupling. *Ann. Rev. Phys. Chem.* **2022**, *73*, 43–71, PMID: 34871038.
- (28) Dunkelberger, A. D.; Simpkins, B. S.; Vurgaftman, I.; Owrutsky, J. C. Vibration-Cavity Polariton Chemistry and Dynamics. *Annu. Rev. Phys. Chem.* **2022**, *73*, 429–451.
- (29) Wright, A. D.; Nelson, J. C.; Weichman, M. L. Rovibrational Polaritons in Gas-Phase Methane. *J. Am. Chem. Soc.* **2023**, *145*, 5982–5987.
- (30) Mandal, A.; Taylor, M.; Weight, B.; Koessler, E.; Li, X.; Huo, P. Theoretical Advances in

- Polariton Chemistry and Molecular Cavity Quantum Electrodynamics. *Chem. Rev.* **2023**, *16*, 9786–9879.
- (31) Fregoni, J.; Garcia-Vidal, F. J.; Feist, J. Theoretical challenges in polaritonic chemistry. *ACS Photonics* **2022**, *9*, 1096–1107.
- (32) Ruggenthaler, M.; Sidler, D.; Rubio, A. Understanding polaritonic chemistry from ab initio quantum electrodynamics. *Chem. Rev.* **2023**, *123*, 11191–11229.
- (33) Foley IV, J. J.; McTague, J.; DePrince III, A. E. *Ab initio* methods for polariton chemistry. *Chem. Phys. Rev* **2023**, *4*, 041301.
- (34) Levine, B. G.; Durden, A. S.; Esch, M. P.; Liang, F.; Shu, Y. CAS without SCF—Why to use CASCI and where to get the orbitals. *J. Chem. Phys.* **2021**, *154*, 090902.
- (35) Shu, Y.; Hohenstein, E. G.; Levine, B. G. Configuration interaction singles natural orbitals: An orbital basis for an efficient and size intensive multireference description of electronic excited states. *J. Chem. Phys.* **2015**, *142*, 024102.
- (36) Fales, B. S.; Shu, Y.; Levine, B. G.; Hohenstein, E. G. Complete active space configuration interaction from state-averaged configuration interaction singles natural orbitals: Analytic first derivatives and derivative coupling vectors. *J. Chem. Phys.* **2017**, *147*, 094104.
- (37) Pijeau, S.; Hohenstein, E. G. Improved Complete Active Space Configuration Interaction Energies with a Simple Correction from Density Functional Theory. *J. Chem. Theor. Comput.* **2017**, *13*, 1130–1146, PMID: 28157312.
- (38) Hu, D.; Huo, P. Ab Initio Molecular Cavity Quantum Electrodynamics Simulations Using Machine Learning Models. *J. Chem. Theory. Comput.* **2023**, *19*, 2353–2368, PMID: 37000936.
- (39) Weight, B. M.; Krauss, T. D.; Huo, P. Investigating Molecular Exciton Polaritons Using Ab

- Initio Cavity Quantum Electrodynamics. *J. Phys. Chem. Lett.* **2023**, *14*, 5901–5913, PMID: 37343178.
- (40) Ruggenthaler, M.; Mackenroth, F.; Bauer, D. Time-dependent Kohn-Sham approach to quantum electrodynamics. *Phys. Rev. A* **2011**, *84*, 042107.
- (41) Ruggenthaler, M.; Flick, J.; Pellegrini, C.; Appel, H.; Tokatly, I. V.; Rubio, A. Quantum-electrodynamical density-functional theory: Bridging quantum optics and electronic-structure theory. *Phys. Rev. A* **2014**, *90*, 012508.
- (42) Pellegrini, C.; Flick, J.; Tokatly, I. V.; Appel, H.; Rubio, A. Optimized Effective Potential for Quantum Electrodynamical Time-Dependent Density Functional Theory. *Phys. Rev. Lett.* **2015**, *115*, 093001.
- (43) Flick, J.; Schäfer, C.; Ruggenthaler, M.; Appel, H.; Rubio, A. Ab Initio Optimized Effective Potentials for Real Molecules in Optical Cavities: Photon Contributions to the Molecular Ground State. *ACS Photonics* **2018**, *5*, 992–1005.
- (44) Jestädt, R.; Ruggenthaler, M.; Oliveira, M. J. T.; Rubio, A.; Appel, H. Light-matter interactions within the Ehrenfest–Maxwell–Pauli–Kohn–Sham framework: fundamentals, implementation, and nano-optical applications. *Advances in Physics* **2019**, *68*, 225–333.
- (45) Flick, J.; Narang, P. Ab initio polaritonic potential-energy surfaces for excited-state nanophotonics and polaritonic chemistry. *J. Chem. Phys.* **2020**, *153*, 094116.
- (46) Vu, N.; McLeod, G. M.; Hanson, K.; DePrince, A. E. I. Enhanced Diastereocontrol via Strong Light–Matter Interactions in an Optical Cavity. *J. Phys. Chem. A* **2022**, *126*, 9303–9312.
- (47) Pavošević, F.; Rubio, A. Wavefunction embedding for molecular polaritons. *J. Chem. Phys.* **2022**, *157*, 094101.
- (48) Liebenthal, M. D.; Vu, N.; DePrince III, A. E. Assessing the Effects of Orbital Relaxation

and the Coherent-State Transformation in Quantum Electrodynamics Density Functional and Coupled-Cluster Theories. *J. Phys. Chem. A* **2023**, *127*, 5264–5275.

- (49) Tokatly, I. V. Time-Dependent Density Functional Theory for Many-Electron Systems Interacting with Cavity Photons. *Phys. Rev. Lett.* **2013**, *110*, 233001.
- (50) Flick, J.; Ruggenthaler, M.; Appel, H.; Rubio, A. Atoms and molecules in cavities, from weak to strong coupling in quantum-electrodynamics (QED) chemistry. *Proc. Natl. Acad. Sci. USA* **2017**, *114*, 3026–3034.
- (51) Tokatly, I. V. Conserving approximations in cavity quantum electrodynamics: Implications for density functional theory of electron-photon systems. *Phys. Rev. B* **2018**, *98*, 235123.
- (52) Malave, J.; Ahrens, A.; Pitagora, D.; Covington, C.; Varga, K. Real-space, real-time approach to quantum-electrodynamical time-dependent density functional theory. *J. Chem. Phys.* **2022**, *157*, 194106.
- (53) Yang, J.; Ou, Q.; Pei, Z.; Wang, H.; Weng, B.; Shuai, Z.; Mullen, K.; Shao, Y. Quantum-electrodynamical time-dependent density functional theory within Gaussian atomic basis. *J. Chem. Phys.* **2021**, *155*, 064107.
- (54) Yang, J.; Pei, Z.; Leon, E. C.; Wickizer, C.; Weng, B.; Mao, Y.; Ou, Q.; Shao, Y. Cavity quantum-electrodynamical time-dependent density functional theory within Gaussian atomic basis. II. Analytic energy gradient. *J. Chem. Phys.* **2022**, *156*, 124104.
- (55) McTague, J.; Foley IV, J. J. Non-Hermitian cavity quantum electrodynamics–configuration interaction singles approach for polaritonic structure with ab initio molecular Hamiltonians. *J. Chem. Phys.* **2022**, *156*, 154103.
- (56) Bauer, M.; Dreuw, A. Perturbation theoretical approaches to strong light–matter coupling in ground and excited electronic states for the description of molecular polaritons. *J. Chem. Phys.* **2023**, *158*, 124128.

- (57) Cui, Z.-H.; Mandal, A.; Reichman, D. R. Variational Lang-Firsov approach plus Moller-Plesset perturbation theory with applications to ab initio polariton chemistry. *arXiv* **2023**,
- (58) Haugland, T. S.; Schäfer, C.; Ronca, E.; Rubio, A.; Koch, H. Intermolecular interactions in optical cavities: An ab initio QED study. *J. Chem. Phys.* **2021**, *154*, 094113.
- (59) Mordovina, U.; Bungey, C.; Appel, H.; Knowles, P. J.; Rubio, A.; Manby, F. R. Polaritonic coupled-cluster theory. *Physical Reviews Research* **2020**, *2*, 023262.
- (60) DePrince, A. E. Cavity-modulated ionization potentials and electron affinities from quantum electrodynamics coupled-cluster theory. *J. Chem. Phys.* **2021**, *154*, 094112.
- (61) Mallory, J. D.; DePrince, A. E. Reduced-density-matrix-based ab initio cavity quantum electrodynamics. *Phys. Rev. A* **2022**, *106*, 053710.
- (62) Weight, B. M.; Tretiak, S.; Zhang, Y. A Diffusion Quantum Monte Carlo Approach to the Polaritonic Ground State. *arXiv* **2023**,
- (63) David Sherrill, C.; Schaefer, H. F. In *The Configuration Interaction Method: Advances in Highly Correlated Approaches*; Löwdin, P.-O., Sabin, J. R., Zerner, M. C., Brändas, E., Eds.; Advances in Quantum Chemistry; Academic Press, 1999; Vol. 34; pp 143–269.
- (64) Olsen, J.; Jørgensen, P.; Simons, J. Passing the one-billion limit in full configuration-interaction (FCI) calculations. *Chem. Phys. Lett.* **1990**, *169*, 463–472.
- (65) Vogiatzis, K. D.; Ma, D.; Olsen, J.; Gagliardi, L.; de Jong, W. A. Pushing configuration-interaction to the limit: Towards massively parallel MCSCF calculations. *J. Chem. Phys.* **2017**, *147*, 184111.
- (66) Abraham, V.; Mayhall, N. J. Selected Configuration Interaction in a Basis of Cluster State Tensor Products. *J. Chem. Theor. Comput.* **2020**, *16*, 6098–6113, PMID: 32846094.
- (67) Park, J. W. Near-Exact CASSCF-Level Geometry Optimization with a Large Active Space using Adaptive Sampling Configuration Interaction Self-Consistent Field Corrected with

- Second-Order Perturbation Theory (ASCI-SCF-PT2). *J. Chem. Theor. Comput.* **2021**, *17*, 4092–4104, PMID: 34096306.
- (68) Guo, Y.; Zhang, N.; Lei, Y.; Liu, W. iCISCF: An Iterative Configuration Interaction-Based Multiconfigurational Self-Consistent Field Theory for Large Active Spaces. *J. Chem. Theor. Comput.* **2021**, *17*, 7545–7561, PMID: 34757746.
- (69) Jeong, W.; Gaggioli, C. A.; Gagliardi, L. Active Learning Configuration Interaction for Excited-State Calculations of Polycyclic Aromatic Hydrocarbons. *J. Chem. Theor. Comput.* **2021**, *17*, 7518–7530, PMID: 34787422.
- (70) Gidofalvi, G.; Mazziotti, D. A. Active-space two-electron reduced-density-matrix method: Complete active-space calculations without diagonalization of the N-electron Hamiltonian. *J. Chem. Phys.* **2008**, *129*, 134108.
- (71) Fosso-Tande, J.; Nguyen, T.-S.; Gidofalvi, G.; DePrince III, A. E. Large-Scale Variational Two-Electron Reduced-Density-Matrix-Driven Complete Active Space Self-Consistent Field Methods. *J. Chem. Theory Comput.* **2016**, *12*, 2260–2271.
- (72) Mullinax, J. W.; Epifanovsky, E.; Gidofalvi, G.; DePrince, A. E. Analytic Energy Gradients for Variational Two-Electron Reduced-Density Matrix Methods within the Density Fitting Approximation. *J. Chem. Theory Comput.* **2019**, *15*, 276–289.
- (73) Maradzike, E.; Hapka, M.; Pernal, K.; DePrince, A. E. Reduced Density Matrix-Driven Complete Active Space Self-Consistent Field Corrected for Dynamic Correlation from the Adiabatic Connection. *J. Chem. Theory Comput.* **2020**, *16*, 4351–4360.
- (74) Mullinax, J. W.; Maradzike, E.; Koulias, L. N.; Mostafanejad, M.; Epifanovsky, E.; Gidofalvi, G.; DePrince, A. E. Heterogeneous CPU + GPU Algorithm for Variational Two-Electron Reduced-Density Matrix-Driven Complete Active-Space Self-Consistent Field Theory. *J. Chem. Theory Comput.* **2019**, *15*, 6164–6178.

- (75) Spohn, H. *Dynamics of charged particles and their radiation field*; Cambridge Univ. Press: Cambridge, 2004.
- (76) Ruggenthaler, M.; Tancogne-Dejean, N.; Flick, J.; Appel, H.; Rubio, A. From a quantum-electrodynamical light–matter description to novel spectroscopies. *Nature Reviews Chemistry* **2018**, *2*, 0118.
- (77) Folkestad, S. D.; Kjørnstad, E. F.; Myhre, R. H.; Andersen, J. H.; Balbi, A.; Coriani, S.; Giovannini, T.; Goletto, L.; Haugland, T. S.; Hutcheson, A.; Høyvik, I.-M.; Moitra, T.; Paul, A. C.; Scavino, M.; Skeidsvoll, A. S.; Tveten, Å. H.; Koch, H. eT 1.0: An open source electronic structure program with emphasis on coupled cluster and multilevel methods. *J. Chem. Phys.* **2020**, *152*, 184103.
- (78) Haugland, T. S.; Ronca, E.; Kjørnstad, E. F.; Rubio, A.; Koch, H. Coupled Cluster Theory for Molecular Polaritons: Changing Ground and Excited States. *Phys. Rev. X* **2020**, *10*, 041043.
- (79) Szabo, A.; Ostlund, N. S. *Modern Quantum Chemistry: Introduction to Advanced Electronic Structure Theory*, 1st ed.; Dover Publications, Inc.: Mineola, 1996.
- (80) Davidson, E. R. The iterative calculation of a few of the lowest eigenvalues and corresponding eigenvectors of large real-symmetric matrices. *Journal of Computational Physics* **1975**, *17*, 87–94.
- (81) Handy, N. Multi-root configuration interaction calculations. *Chemical Physics Letters* **1980**, *74*, 280–283.
- (82) Olsen, J.; Roos, B. O.; Jørgensen, P.; Jensen, H. J. A. Determinant based configuration interaction algorithms for complete and restricted configuration interaction spaces. *The Journal of Chemical Physics* **1988**, *89*, 2185–2192.
- (83) Vogiatzis, K. D.; Ma, D.; Olsen, J.; Gagliardi, L.; de Jong, W. A. Pushing configuration-

- interaction to the limit: Towards massively parallel MCSCF calculations. *The Journal of Chemical Physics* **2017**, *147*, 184111.
- (84) Knowles, P. J.; Handy, N. C. A determinant based full configuration interaction program. *Computer Physics Communications* **1989**, *54*, 75–83.
- (85) Bendikov, M.; Duong, H. M.; Starkey, K.; Houk, K. N.; Carter, E. A.; Wudl, F. Oligoacenes: Theoretical Prediction of Open-Shell Singlet Diradical Ground States. *J. Amer. Chem. Soc.* **2004**, *126*, 7416–7417, PMID: 15198569.
- (86) Hachmann, J.; Dorando, J. J.; Avilés, M.; Chan, G. K.-L. The radical character of the acenes: A density matrix renormalization group study. *J. Chem. Phys* **2007**, *127*, 134309.
- (87) Qu, Z.; Zhang, D.; Liu, C.; Jiang, Y. Open-Shell Ground State of Polyacenes: A Valence Bond Study. *J. Phys. Chem. A* **2009**, *113*, 7909–7914, PMID: 19527036.
- (88) Fosso-Tande, J.; Nascimento, D. R.; DePrince III, A. E. Accuracy of two-particle N-representability conditions for describing different spin states and the singlet-triplet gap in the linear acene series. *Mol. Phys.* **2016**, *114*, 423–430.
- (89) Martínez-Martínez, L. A.; Du, M.; Ribeiro, R. F.; Kéna-Cohen, S.; Yuen-Zhou, J. Polariton-Assisted Singlet Fission in Acene Aggregates. *J. Phys. Chem. Lett.* **2018**, *9*, 1951–1957.
- (90) Eizner, E.; Martínez-Martínez, L. A.; Yuen-Zhou, J.; Kéna-Cohen, S. Inverting singlet and triplet excited states using strong light-matter coupling. *Science Advances* **2019**, *5*, eaax4482.

TOC Graphic

